COMPARING CONTIGUOUS AND DISCONTIGUOUS ENERGY GRIDS AND PROPAGATING UNCERTAINTIES FOR RADIATION TRANSPORT FINITE ELEMENT METHODS

A Thesis

by

PABLO A. VAQUER

Submitted to the Office of Graduate and Professional Studies of
Texas A&M University
in partial fulfillment of the requirements for the degree of

MASTER OF SCIENCE

Chair of Committee,	Ryan G. McClarren
Committee Members,	Marvin L. Adams
	Raytcho Lazarov
Head of Department,	Yassin A. Hassan

December 2016

Major Subject: Nuclear Engineering

ABSTRACT

The purpose of this study is to quantitatively compare the accuracy of radiation transport finite element methods which use a contiguous support to those which use a discontiguous support of the energy domain. The finite-element-with-discontiguous-support method (FEDS) is a generalized finite element framework for discretizing the energy domain of radiation transport simulations. FEDS first decomposes the energy domain into coarse groups and then further partitions the coarse groups into discontiguous energy elements within each coarse group. A minimization problem is solved in order to optimally cluster poritions of the energy domain into FEDS elements.

This document presents a procedure for propagating uncertainties for FEDS, and afterwards presents four benchmark problems that test the efficacy of FEDS, compared to Multigroup, for different radiation transport problems. The results from these benchmark problems suggest that we are accurately generating FEDS cross sections, correctly propating uncertainties from the nuclear data libraries, and that FEDS converges faster than Multigroup to an energy-resolved solution. The absolute error in the verification problems were 6×10^{-8} and 5×10^{-8}, respectively, and the absolute error in the validation problems were 2×10^{-4}, and 4×10^{-3}, respectively.

ACKNOWLEDGEMENTS

I would like to express my gratitude towards a few individuals who helped make this work possible. First, I would like to thank my mentor, Dr. Ryan McClarren. for his continual guidance throughout the course of this research project.

I would also like to thank Dr. Teresa Bailey, Dr. Peter Brown, and Dr. Robert Cavallo at LLNL for openly discussing the challenges of this project as well as providing me path forward in this research.

In addition, I would like express my gratitude towards many of fellow graduate students at Texas A&M University. In particular, I would like thank Andrew Till and Donald Bruss for providing me several Python scripts which I leveraged for this study as well as their willingness to thoroughly answer any questions I had during the course of this research. I would also like to thank William D. Hawkins for helping me debug errors I encountered with PDT, and Stephen Revis for helping me convert my MCNP6 geometry to a discretized PDT geometry. Also, I would like to thank Steven Horowitz, Simon Bolding, Aaron Holzaepfel, Jacob Landman, Tarek Ghaddar and Daniel Holladay for the experiences we shared throughout grad school.

Most importantly, I would like to express my gratefulness to my family. I would like to thank my parents, Patricia Vettorello and Pablo Vaquer, and my big sister, Vanesa Vaquer, for their love, support, advice, and encouragement.

NOMENCLATURE

ACE	A Compact ENDF
ENDF	Evaluated Nuclear Data File
FEDS	Finite Element with Discontiguous Support
GENDF	Groupwise ENDF
MCNP	Monte Carlo N-Particle Transport Code
MG	Multigroup
NJOY	Nuclear Data Processing System
PENDF	Pointwise ENDF
PDT	Parallel Deterministic Transport Code
RRR	Resolved Resonance Region
S_N	Discrete Ordinates
URR	Unresolved Resonance Region
Q	Quantity of Interest

TABLE OF CONTENTS

Page

LIST OF FIGURES

LIST OF TABLES

TABLE Page

1. INTRODUCTION

The general form of the neutral-particle transport equation can be written as

$$\frac{1}{v(E)}\frac{\partial\psi}{\partial t} + \hat{\Omega}\cdot\nabla\psi + \Sigma_t(\vec{r},E,t)\psi(\vec{r},\hat{\Omega},E,t) = s(\vec{r},\hat{\Omega},E,t), \tag{1.1}$$

where

$\vec{r}$	position of particles in space $< x, y, z >$
$\hat{\Omega}$	particles' direction of travel $< \theta, \varphi >$
E	kinetic energy of particles
t	time
$v(E)$	particles' speed
$\psi(\vec{r},\hat{\Omega},E,t)$	angular flux
$\Sigma_t(\vec{r},E,t)$	total macroscopic cross section
$s(\vec{r},\hat{\Omega},E,t)$	source term (includes scattering, fission, etc.)

While this equation may seem relatively simplistic, the intricacies are buried into the energy dependence of cross sections as well as the source term. The energy dependence of cross sections can be complex due to nuclear resonances, a quantum mechanical effect which can cause nuclear cross sections to vary by several orders of magnitude due to a small change in incident particle energy. Figure 1.1 shows how nuclear cross sections vary on a logarithmic scale.

Deterministic methods try to solve Eq.(1.1) by discretizing the six-dimensional phase space $\vec{r}$, $\hat{\Omega}$, and E, as well as time t. However, this requires lots of computer memory due its large dimensionality, and deterministic codes are forced to find a balance between coarse and fine discretizations of the space, angle, energy and time.

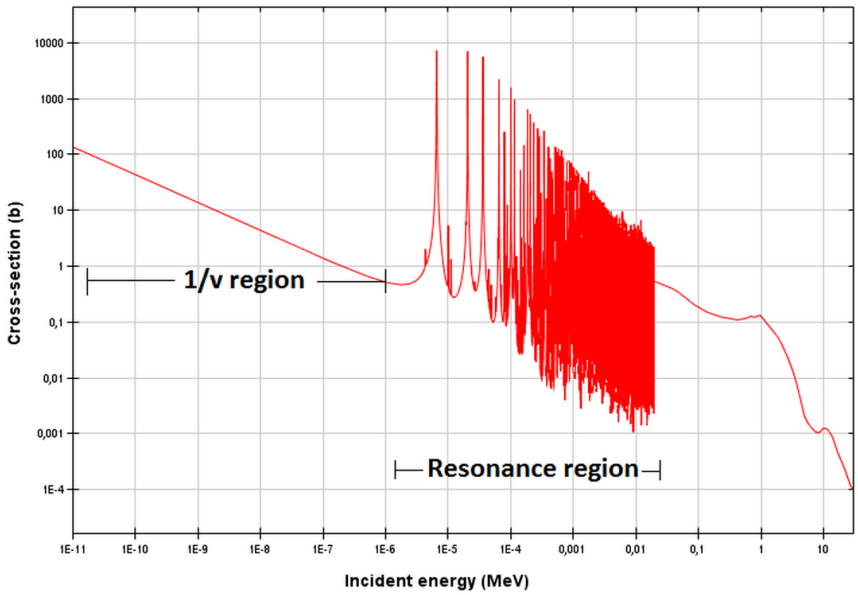

Figure 1.1: Microscopic total cross section for ^{238}U.

A deterministic method known as the Multigroup method attempts to solve Eq.(1.1) by discretizing the energy domain into several contiguous energy intervals called groups, such that

$$\Delta E_g \equiv \{E | E \in [E_{g-1}, E_g)\} \, ,$$

where g represents an energy group. Afterwards, group cross sections Σ_g are computed by weighting the cross section as a function of energy $\Sigma(E)$ by an arbitrary function $w(E)$, as shown below

$$\Sigma_g = \int_{E_{g-1}}^{E_g} dE \, w(E) \Sigma(E) \, .$$

Here $w(E)$ is assumed to have the distribution in energy as the angular flux $\psi(E)$. Cross sections are weighted in this manner in order to conserve reaction rates. The problem with this weighting technique is that the angular flux is still unknown at this point. Thus the weighting function $w(E)$ may not be similar enough to $\psi(\vec{r}, \hat{\Omega}, E)$ in order to properly

conserve reaction rates. The angular flux may vary widely in different regions of the problem and as a function of angle. In addition, nuclear resonances in different materials don't necessarily fall within the same energy bins, thus a group mesh that works well with one material doesn't necessarily work well with all materials. Often, the only way to obtain an accurate radiation transport simulation is to use very fine groups, but this is rarely feasible due to computer memory constraints.

In the 1960's Nikolaev [2][3] and Stewart [4] proposed using Multiband for neutron and photon transport. Multiband is a method which discretizes the energy domain into discontiguous energy bands according to the magnitude of the cross section, rather than contiguous energy groups. An example of these discontiguous energy bands is shown in Fig.(1.2). This method is capable of capturing the effect of multiple resonances simultaneously while reducing memory costs. Recently, Till, Morel, and Adams [5] have acknowledged the advantages and disadvantages of Multigroup and Multiband to introduce a generalized finite element framework known as the finite-element-with-discontiguous-support (FEDS) Multigroup method. FEDS combines elements of both Multigroup and Multiband. FEDS first splits up the energy domain into coarse groups, and then clusters small discontiguous energy segments into energy elements within each coarse group. This is done by representing the particle flux as a linear combination of basis functions that have a discontiguous support in energy. An example of how FEDS partitions the energy domain is shown in Fig.(1.3).

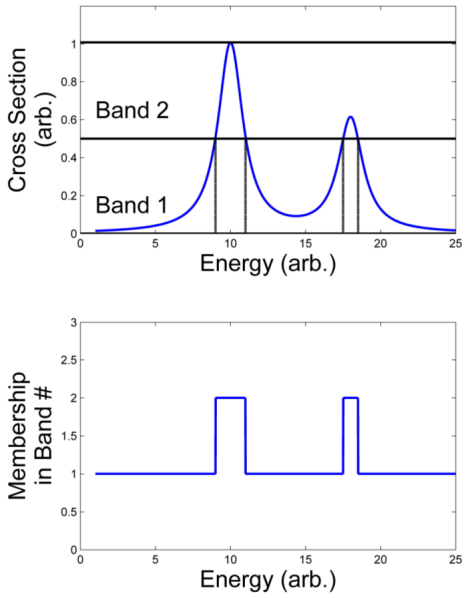

Figure 1.2: An example of the Multiband method with only two bands [1].

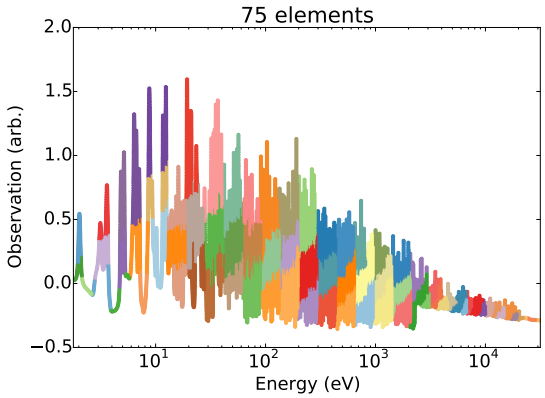

Figure 1.3: An example of FEDS with 75 elements. Each color represents a separate energy element. "Observation" refers to the logarithm of the scalar flux.

The purpose of this study is to quantitatively compare the accuracy of radiation transport finite element methods which use a contiguous support to those which use a discontiguous support of the energy domain. This document presents a procedure for propagating uncertainties for FEDS, and afterwards presents four benchmark problems that will test the efficacy of FEDS for different radiation transport problems. Specifically, this study uses NJOY 2012 along with a python script to read cross sections from the ENDF/B-VII.1 nuclear data library to generate a covariance matrix for a given discontiguous energy domain. The covariance matrix along with the sensitivities of a quantity of interest to different parameters are then used to calculate the variance of the quantity of interest.

2. THEORY

In this section we start by discussing the differences between Multigroup and FEDS cross sections. Then, we describe how to generate Multigroup and FEDS cross sections using the Bondarenko method. Then, we highlight the differences between generating accurate cross sections for fast-spectrum and thermal-spectrum systems. Lastly, we demonstrate how to propagate uncertainties for FEDS.

2.1 FEDS vs. Multigroup

The Multigroup method requires that the support for each group is contiguous. For example, if particle energies of 1 eV and 3 eV both fall within the energy range of a single group, then particles of energy 2 eV must also belong to that energy group. In FEDS, groups are split up further into energy elements, but the support for these energy elements does not necessarily have to be contiguous within each group. A single element can be composed of several discontiguous subelements, however all subelements that belong to a single element must fall within the energy range of a single coarse group. Returning to our previous example, in FEDS, if energies of 1 eV and 3 eV belong to an element, the energy 2 eV may or may not belong to that same element. Figure 2.1 demonstrates how coarse groups can be composed of several elements. Figure 2.1 also shows that elements can be composed of tens or hundreds of discontiguous subelements in the resolved-resonance range (RRR).

The idea behind FEDS is to minimize how much the particle flux varies within a single element. This is not a simple minization problem, because the particle flux can vary drastically, even within the same material in a problem. For example, the neutron energy spectrum in the center of a fuel rod in a reactor is not the same as the neutron spectrum at the edge of the fuel rod. Thus, we first select a set of spectra that we want our finite

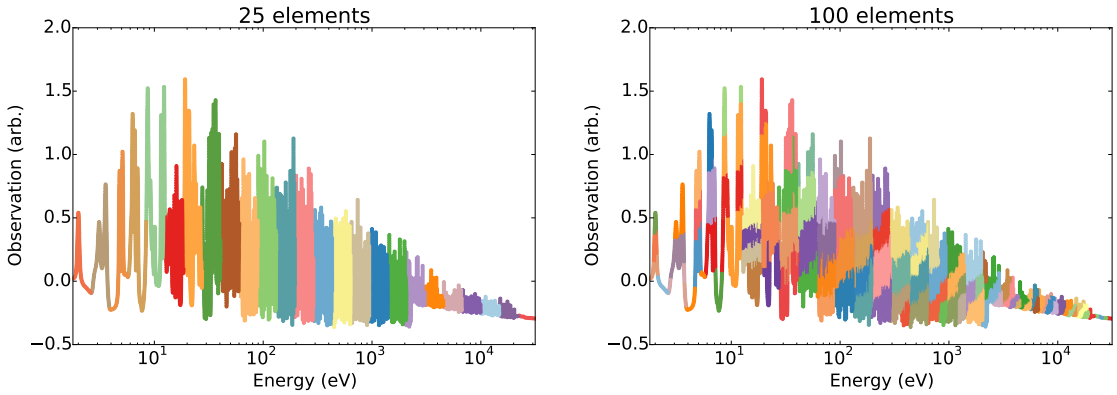

(a) 25 energy groups in RRR

(b) 100 energy elements in RRR

Figure 2.1: These plots show the difference between Multigroup and FEDS. In the left plot, each color represents a different energy group. In the right plot, each of the 25 coarse group contains 4 FEDS energy elements for a total of 100 elements in the resolved-resonance range (RRR), and each color represents a different element.

element space to accurately represent. Then the following minimization problem can be solved to generate an optimal energy element mesh:

1. Given a set of spectra and energy subelements, arbitrarily map subelements into elements.

2. Compute the averages of the spectra in each element.

3. Compute the difference between the continuous-energy spectrum and the element-averaged spectrum, and sum these differences over all elements and spectra. We will refer to this total difference as the *variance error*.

4. Choose the energy element mesh which minimizes the variance error by looking at all possible combinations of subelements into elements.

This variance error essentially measures the accuracy of resonance-scale behavior that is captured using a particular energy element mesh. There are several machine-learning algo-

rithms for clustering subelements into elements, and iterating over possible combinations of subelements into elements to generate an optimal FEDS energy grid. These algorithms are discussed in detail by Till in [5].

A generalized Petrov-Galerkin finite element method can be defined for these discontiguous energy elements as

$$\varphi(\vec{r},\hat{\Omega},E) \equiv \sum_{e=1}^{N_e} \Psi_e(\vec{r},\hat{\Omega}) b_e(\vec{r},E) \tag{2.1}$$

where

$$b_e(\vec{r},E) = \begin{cases} \frac{f_i(E)}{\int_{E_e} dE\, f_i(E)} & \text{if } E \in E_e, \\ 0 & \text{otherwise,} \end{cases} \tag{2.2}$$

and

$$w_e(E) = \begin{cases} 1 & \text{if } E \in E_e, \\ 0 & \text{otherwise.} \end{cases} \tag{2.3}$$

By substituting this basis-function representation of the angular flux into the transport equation, one can derive the FEDS transport equation,

$$\left[\hat{\Omega}\cdot\nabla + \Sigma_{t,e}(\vec{r})\right]\Psi_e(\vec{r},\hat{\Omega}) = \sum_{\ell=0}^{L}\sum_{m=-\ell}^{\ell} \frac{2\ell+1}{4\pi} Y_\ell^m(\hat{\Omega}) \sum_{e'=1} \Sigma_{s,\ell,e'\to e}(\vec{r})\Phi_{\ell,e'}^m(\vec{r}) + \frac{\chi_e(\vec{r})}{4\pi k}\sum_{e'=1}\nu\Sigma_{f,e'}(\vec{r})\Phi_{e'}(\vec{r})\,. \tag{2.4}$$

Notice, that the FEDS transport equation is very similar to the Multigroup equation with the exception that the energy elements, e, are computed as weighted averages over the discontiguous support of the energy elements. The advantage in solving the FEDS transport equation over the Multigroup equation is that the FEDS elements are theoretically

better at capturing resonance-scale behavior. However, the FEDS transport equation is more computationally expensive because the scattering matrix can be more dense in the resolved-resonance region (RRR) (namely, there can be lots of up- and down-scattering between different elements in the RRR).

2.2 Bondarenko Method

In order to generate FEDS or Multigroup microscopic cross sections, the spectrum of particle energies must be known first, and spectra can vary widely for different geometries and materials. In our best attempt to preserve reaction rates in all space and directions, we begin with the steady-state transport equation

$$\hat{\Omega} \cdot \nabla \psi + \Sigma_t(\vec{r}, E)\psi(\vec{r}, \hat{\Omega}, E) = s(\vec{r}, \hat{\Omega}, E) \tag{2.5}$$

and integrate over all $\vec{r}$ and $\hat{\Omega}$ to get

$$J^+(E) - J^-(E) + \Sigma_t(E)\phi(E) = s(E)\,, \tag{2.6}$$

where

$\phi(E)$ scalar flux
$J^-(E)$ outward particle current
$J^+(E)$ inward particle current .

In order to solve for the flux we can make the following substitutions

$$\Sigma_e(E) = \frac{J^+(E)}{\phi(E)} \quad \text{and} \quad S(E) = s(E) + J^-(E)$$

and show that

$$\phi(E) \approx \frac{S(E)}{\Sigma_e + \Sigma_t(E)} \tag{2.7}$$

where $S(E)$ is the modified source rate which includes the inward particle current, and Σ_e is the escape cross section which takes leakage into account. There are many ways to approximate an escape cross section. For simplicity, in this study we approximated the escape cross section as the inverse of the mean chord length of a material's geometry.

The purpose of obtaining a simplified solution for the scalar flux is to be able obtain a decent weighting function for producing Multigroup or FEDS cross sections,

$$w(E) \approx \frac{S(E)}{\Sigma_e + \Sigma_t(E)} \,. \tag{2.8}$$

However, at this point $\Sigma_t(E)$ is still unknown. Therefore we must iterate to obtain our values for $w(E)$ and $\Sigma_t(E)$. Cross-section-generation codes typically produce microscopic cross sections for each isotopes separately, thus we can make the following substitution

$$\sigma_{0,i}(E) = \frac{1}{N_i}\Big(\Sigma_e + \sum_{j \neq i} N_j \sigma_{t,j}^{k-1}(E)\Big) \,,$$

to rewrite Eq.(2.8) in terms of microscopic cross sections,

$$w_i(E) \approx \frac{S(E)}{N_i\Big(\sigma_{t,i}(E) + \sigma_{0,i}(E)\Big)} \,,$$

where $\sigma_{t,i}$ is the total microscopic cross section for isotope i and $\sigma_{0,i}$ is the background cross section for isotope i. The background cross section includes any particle loss that is not caused by isotope i.

Bondarenko iterations can be used to produce self-consistent FEDS or Multigroup microscopic cross sections for each energy group and each isotope in a material. A Bondarenko iteration consists of the following steps:

1. Calculate the background cross section $\sigma^k_{0,g,i}$ for iteration k,

$$\sigma^k_{0,g,i} = \frac{1}{N_i}\Big(\Sigma_e + \sum_{j\neq i} N_j \sigma^{k-1}_{t,g,j}\Big) \, .$$

   In the first iteration the value of $\sigma^k_{0,g,i}$ is guessed.

2. Compute the weighting spectrum, based on the new background cross section,

$$w^k_i(E) \approx \frac{S(E)}{N_i\big(\sigma^k_{t,g,i} + \sigma^k_{0,g,i}\big)} \, .$$

3. Compute the total cross section $\sigma^k_{t,g,i}$ for isotope i using the new weighting spectrum,

$$\sigma^k_{t,g,i} = \frac{\int_{E_g}^{E_{g-1}} dE \, w^k_i(E)\sigma^k_{t,i}(E)}{\int_{E_g}^{E_{g-1}} dE \, w^k_i(E)} \, .$$

   Do this for all isotopes and groups.

4. Check if the following convergence criterion is satisfied,

$$\left|\left| \frac{\sigma^k_{t,g,i} - \sigma^{k-1}_{t,g,i}}{\sigma^k_{t,g,i}} \right|\right|_{L^\infty} < \epsilon \, .$$

   If the convergence criterion is not satisfied, return to step 1 using the updated values for $\sigma^{k-1}_{t,g,j}$.

For FEDS, replace group g with element e.

2.3 Uncertain Parameters in Neutron Transport

For this portion of the theory section, we will limit our discussion to propagating uncertainties for the steady-state form of the neutron transport equation. The detailed form

of Eq.(1.1) for steady-state neutron transport is

$$\hat{\Omega}\cdot\nabla\psi+\Sigma_t(\vec{r},E)\psi(\vec{r},\hat{\Omega},E)= \int_{4\pi}d\Omega'\int_0^\infty dE'\,\Sigma_s(\vec{r},\hat{\Omega}'\cdot\hat{\Omega},E'\rightarrow E)\psi(\vec{r},\hat{\Omega}',E')+ \frac{1}{k_{\text{eff}}}\frac{1}{4\pi}\int_0^\infty dE'\,\Sigma_f(\vec{r},E'\rightarrow E)\psi(\vec{r},\hat{\Omega}',E') \quad (2.9)$$

and

$$\psi(\vec{r},\hat{\Omega},E,t)=f(\vec{r},\hat{\Omega},E,t)\quad \text{for } r\in\partial V,\ \hat{\Omega}\cdot\hat{n}<0\,.$$

where the macroscopic cross section Σ_x for reaction x is the sum of microscopic cross section $\sigma_{i,x}$ of the constituent isotopes, weighted by the number densities of those isotope N_i,

$$\Sigma_x=\sum_{i=1}^{I}N_i\sigma_{i,x}$$

In Eq.(2.9), the fission source term contains a double-differential fission cross section $\Sigma_f(\vec{r},E'\rightarrow E)$ (which is similar to a double-differential scattering cross section, except multiple neutrons can be produced per fission). This fission source term is physically accurate because the number of neutrons produced per fission and the energy of those neutrons is dependent on the incident neutron energy. However, it's important to note that typically the following approximation is made for the fission source term

$$\int_0^\infty dE'\,\Sigma_f(\vec{r},E'\rightarrow E)\psi(\vec{r},\hat{\Omega}',E')\approx\chi(E)\int_0^\infty dE'\,\nu\Sigma_f(\vec{r},E')\psi(\vec{r},\hat{\Omega}',E')\,. \quad (2.10)$$

Together Eq.(2.9) and Eq.(2.10) contain several uncertain parameters:

N_i	number density of isotope i
$\sigma_{t,i}(\vec{r}, E)$	total microscopic cross section for isotope i
$\sigma_{s,i}(\vec{r}, \hat{\Omega}' \cdot \hat{\Omega}, E' \rightarrow E)$	double-differential scattering cross section for isotope i
$\chi_i(E)$	spectrum of neutron energies produced from fission
$\nu_i(\vec{r}, E')$	number of neutrons produced per fission
$\sigma_{f,i}(\vec{r}, E')$	fission cross section
∂V	location of boundary or interface
$f(\vec{r}, \hat{\Omega}, E)$	boundary condition

In order to properly propagate uncertainties, we need more than just the standard deviation of the uncertainty of each uncertain parameter. We also need the covariance between all uncertain parameters. The covariances between different isotopes at different energies are computed based on experimental data. The covariance between two parameters p_i and p_j is defined as

$$\text{cov}(p_i, p_j) = \langle p_i p_j \rangle - \langle p_i \rangle \langle p_j \rangle \, , \tag{2.11}$$

where $\langle \cdot \rangle$ is used to represent expected value. The covariance between all uncertain parameters can be represented by a covariance matrix. However, constructing a covariance matrix for all uncertain parameters is computationally expensive, and may be unnecessary since many parameters are uncorrelated.

We can reduce the size of the covariance matrix by assuming there is no correlation between the cross sections of different materials. This results in each material having it's own separate covariance matrix. While this assumption is valid for most materials, it is not the case for all materials. Furthermore, we can greatly reduce the size of this covariance matrix by determining the covariance between scattering cross sections (instead of double-

differential scattering cross sections) by using the property

$$\text{cov}(\sigma_{s,g}, \sigma_{s,g}) = \sum_{g'=1}^{G} \sum_{g''=1}^{G} \text{cov}(\sigma_{s,g\to g'}, \sigma_{s,g\to g''}) \tag{2.12}$$

and compute sensitivity of the quantity of interest Q to $\sigma_{s,\ell,g}$ using the following relation was derived by Bruss in [6],

$$\frac{\partial Q}{\partial \sigma_{s,\ell,g}} = \sum_{g'=1}^{G} \frac{\partial Q}{\partial \sigma_{s,\ell,g}} \frac{\sigma_{s,\ell,g\to g'}}{\sigma_{s,g}} \, . \tag{2.13}$$

2.4 Uncertainty Propagation for FEDS

In order to propagate uncertainties for FEDS, we will first define the variance in some quantity of interest Q as

$$\text{var}(Q) = \sum_{i=1}^{P} \sum_{j=1}^{P} \frac{\partial Q}{\partial p_i} \frac{\partial Q}{\partial p_j} \text{cov}(p_i, p_j) \tag{2.14}$$

where p is used to represent any parameter which may affect the quantity of interest, and P is the total number of relevant parameters. These parameters can be cross sections for different interactions, at different incident-particle energies, in different materials as well as many other uncertain parameters. It is important to consider than if a fine energy grid is used for a simulation, the covariance matrix will be massive (especially if one includes the covariance between all the elements of double-differential scattering matrices of different Legendre-order).

Note that the value of $\text{cov}(p_i, p_j)$ could have some uncertainty itself which isn't being considered in Eq.(2.14). Also, Eq.(2.14) doesn't not consider high-order sensitivities of the quantity of interest (such as $\partial^2 Q/\partial p_i^2$) which may be important for some uncertainty calculations.

Now, in order to derive a general covariance matrix for FEDS let us first assume p_i and p_j are parameters composed of a discontiguous set of parameters,

$$p_i = \{\theta_{i,1}, \theta_{i,2}, \ \ldots, \theta_{i,M}\}$$

$$p_j = \{\theta_{j,1}, \theta_{j,2}, \ \ldots, \theta_{j,N}\} \ .$$

Henceforth, we will refer to p_i and p_j as elements and $\theta_{i,m}$ and $\theta_{j,n}$ as subelements. Now by using the additive law of covariance,

$$\text{cov}(X + Y, Z) = \text{cov}(X, Z) + \text{cov}(Y, Z) \ .$$

we can show that covariance between two elements is simply the sum of the covariances of their subelements,

$$\text{cov}(p_i, p_j) = \sum_{m=1}^{M} \sum_{n=1}^{N} \text{cov}(\theta_{i,m}, \theta_{j,n}) \ , \tag{2.15}$$

where M and N represent the total number of subelements that belong to elements i and j, respectively. Thus, by combining Eq.(2.14) and Eq.(2.15) we get that the variance in the quantity of interest for FEDS is equal to

$$\boxed{\text{var}(Q) = \sum_{i=1}^{P} \sum_{j=1}^{P} \frac{\partial Q}{\partial p_i} \frac{\partial Q}{\partial p_j} \left\{ \sum_{m=1}^{M} \sum_{n=1}^{N} \text{cov}(\theta_{i,m}, \theta_{j,n}) \right\}} \ . \tag{2.16}$$

Figure 2.2 shows an example of an element correlation matrix and it's corresponding subelement correlation matrix.

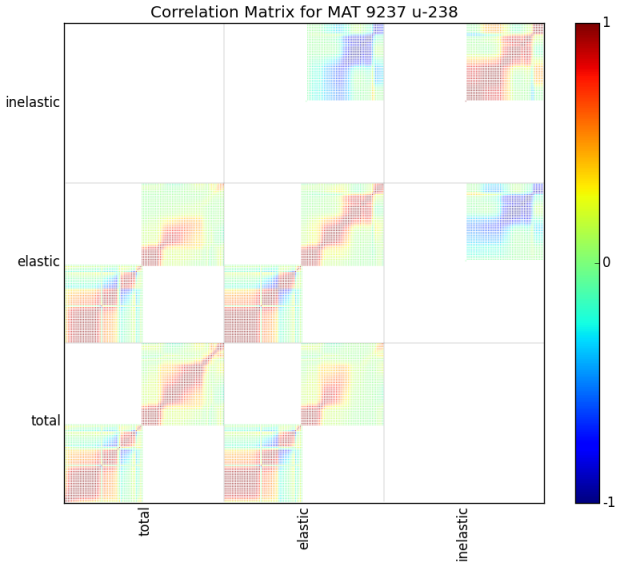

(a) Subelement correlation matrix

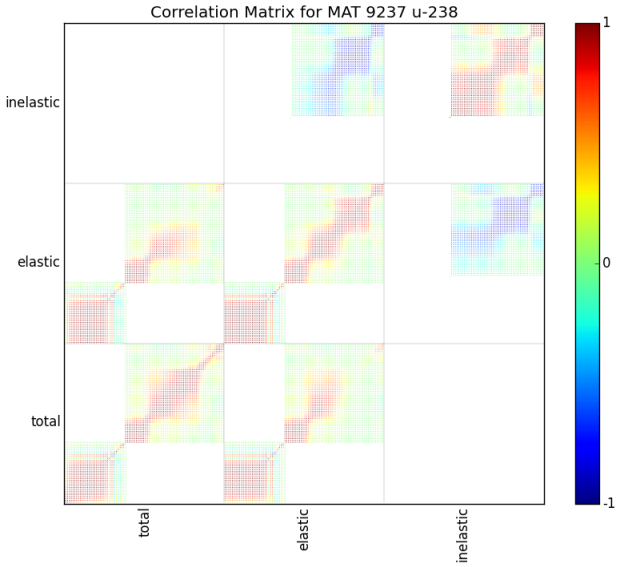

(b) Element correlation matrix

Figure 2.2: Comparison of subelement correlation matrix and an corresponding element correlation matrix for ^{238}U generated using Barnfire for a coarse energy mesh. A correlation matrix is simply a normalized covariance matrix.

3. IMPLEMENTATION

A cross section generation framework known as Barnfire was developed at Texas A&M University to generate both Multigroup and FEDS cross sections, and propagate uncertainties for radiation transport problems. Barnfire is primarily a collection of python scripts that manipulate nuclear data, but it can also run the Nuclear Data Processing System (NJOY) [7] and Parallel Deterministic Transport (PDT) [8]. NJOY is a tool for producing pointwise and Multigroup cross sections, while PDT is a discrete-ordinates (S_N) radiation-transport code currently being developed at Texas A&M University.

During the course of this research project, the capabilities of Barnfire were extended to allow the user to:

- Control subelement-width size when creating group mesh with discontiguous-support
- Produce different "escape" cross section approximations for different geometries
- Produce a more accurate fission spectrum $\chi(E)$
- Easily change the weighting spectrum used by the GROUPR module of NJOY
- Parse PDT input files, cross section files, and output files
- Generate PDT cross section files (compatible with PDT's adjoint mode)
- Generate FEDS covariance matrices for different materials
- Calculate the variance in the quantity of interest

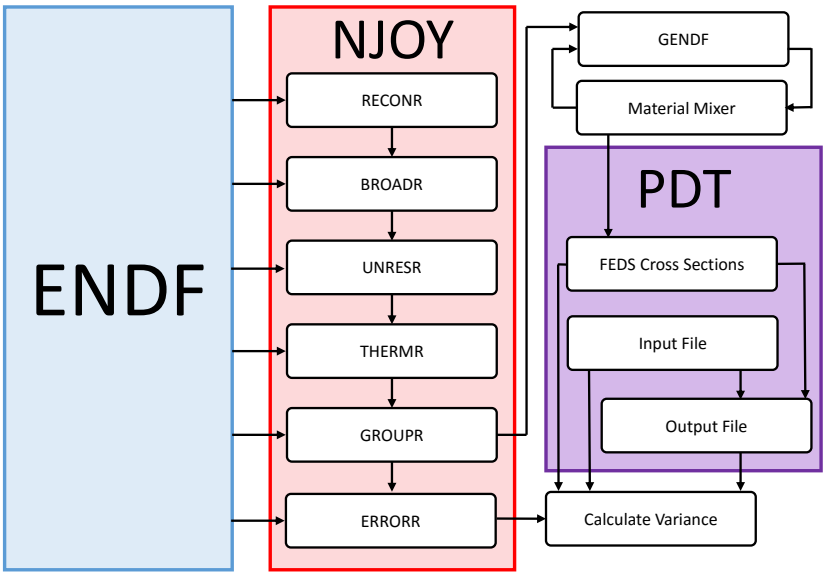

Figure 3.1: This flow chart demonstrate how NJOY and PDT are integrated into Barnfire for generating Multigroup or FEDS cross sections as well as propagating uncertainties from nuclear data.

Figure 3.1 demonstrates most of Barnfire's current capabilities and code structure. The NJOY modules (RECONR, BROADR, UNRESR, THERMR, GROUPR, and ERROR) collect data stored in Evaluated Nuclear Data Format (ENDF) files to construct cross sections and covariance matrices. These NJOY modules allow for a high level of cross section customization, because the user can provide accurate weighting fluxes, material temperatures, thermal treatments, and several other physical parameters. NJOY then outputs a groupwise ENDF (GENDF) file which contains Multigroup cross sections (or in this case subelement cross sections).

Note that at this point the subelement cross sections stored in the GENDF file are still inaccurate because the weighting spectrum used in NJOY does not include resonance self-shielding effects. The resonances of all the isotopes in a material, as well as the geometry of material, affect the neutron spectrum. *Bondarenko iterations* are used to mix different

materials as well as account for leakage in order to generate a more accurate weighting spectrum for that material.

Afterwards, Barnfire collapses the FEDS subelement cross sections into FEDS element cross sections and produces a PDT cross section file for each isotope in the problem. Next, a PDT input file along with the previously-generated cross section files are used to run PDT and determine a quantity of interest Q and corresponding sensitivities $\partial Q/\partial p_i$ for each parameter p_i.

Finally, Barnfire collapses the subelement covariance matrix for each isotope into element covariance matrices. The element covariance matrices along with the sensitivities computed with PDT are used to determine the variance in the quantity of interest.

3.1 Generating Pointwise Cross Sections

Most Monte Carlo codes (such as MCNP6) are capable of handling continuous-energy cross sections [9]. Instead of solving a discretized form of the transport equation, Monte Carlo codes sample probability distribution functions to determine the likelihood of different nuclear reactions such as fission, scattering, and capture reactions. MCNP6 is capable of acquiring the unique cross section value according to a particle's energy, by reading in pointwise cross sections (which contains greater than 100,000 cross section values corresponding to different particle energies) and logarithmically interpolates to obtain the value of the cross section at some particular energy. MCNP6 requires that this pointwise cross section library be stored in the ACE format.

Fortunately, Barnfire is capable of producing customized ACE files using NJOY. One starts by creating a python class for a material, including material properties such as isotopic composition, elemental composition, mass density, temperature, and thermal treatment. These material specifications are then used to create NJOY input files for each isotope in the problem. NJOY is then used to generate a pointwise ENDF (PENDF) file.

Afterwards, the ACER module of NJOY reads the PENDF file and converts the pointwise cross section data to A Compact ENDF (ACE) format.

3.2 Generating FEDS Cross Sections

As derived in the Theory section, the FEDS transport equation is identical to the Multigroup transport equation. Thus, FEDS cross section data and Multigroup cross section data are both stored in the usual PDT cross section format. However, the process of generating FEDS cross sections is very convoluted.

One starts by creating a python class for a material in Barnfire, which includes any material specifications. A material can contain several elements and several isotopes per element. Barnfire then generates a NJOY input file for each isotope in the material and runs NJOY to generate PENDF files.

Barnfire then generates a subelement mesh. The subelement mesh is essentially a Multigroup mesh containing thousands of energy bins within the resolved resonance range (RRR). Afterwards the energy subelements are clustered into energy elements using a machine-learning clustering algorithm, and minimizes the variation of the spectrum within each energy element such that each energy element can be well-characterized by a single cross section value. Recall that each energy elements can be discontiguous. Barnfire was recently modified to set a minimum subelement-width size, so that the upper energy bound for a subelement was at least 1.0001 times larger than the lower energy bound for that subelement (this was done to prevent the ERRORR module of NJOY from crashing, however it hinders Barnfire's ability to produce an optimal element mesh in the RRR).

Next, the GROUPR module of NJOY is used along with the subelement group mesh and a weighting spectrum to generate a GENDF file. The GENDF file contains the subelement cross sections for several different nuclear reactions. Although, occasionally nuclear reactions may be missing from the GENDF file and need to be added manually.

At this point, Bondarenko iterations are used mix different materials to generate a more accurate weighting spectrum for that material. Barnfire was recently update to handle different material geometries by computing a geometry-dependent escape cross section and modifying the weighting spectrum accordingly. Barnfire then collapses the subelement cross sections into element cross sections. This is similar to how a fine-group mesh can be collapsed into a coarse-group mesh, except elements can be discontiguous. Finally, Barnfire produces a PDT cross section file for each isotope in the problem.

3.3 Propagating Uncertainties for PDT

PDT can compute the quantity of interest Q and sensitivities $\partial Q/\partial p_i$ to several parameters p_i [10]. PDT currently provides the option to compute one of three quantities of interest, shown in Table 1. PDT provides the sensitivity of the chosen quantity of interest to the parameters shown in Table 2.

Table 3.1: PDT's options for quantity of interest

Quantity of interest	PDT variable name
N	`TotalInventoryQOI`
$\langle N\sigma, \psi \rangle$	`ReactionRateQOI`
ρ	`ReactivitiyQOI`

Table 3.2: Available parameters for PDT sensitivity estimates

Parameter	PDT variable name
σ_t	`sigma T`
σ_s	`sigma S`
$\nu\sigma_f$	`NU sigma F`
σ_f	`sigma F`
ν	`NU`
λ	`DECAY CONSTANT`
N_o	`INITIAL DENSITY`

PDT compute sensitivities using forward-adjoint perturbation theory estimates [10]. The benefit of this approach is PDT can solve the forward and adjoint transport equations once and obtain the sensitivities of all the relevant parameters, instead of having doing direct perturbation and having to run the code multiple times for each parameter.

Running PDT in forward-adjoint mode requires specific nuclear reactions to be included in all PDT cross section files, regardless of whether they are necessary for the simulation or if the value for that parameter is zero. The nuclear reactions that must be included in PDT cross section files are listed in Table 3.

Table 3.3: Necessary parameters in PDT cross section files

Parameter	MT number
σ_t	1
σ_{el}	2
σ_{inel}	4
σ_f	18
ν	452
$\nu\sigma_f$	1452
χ	1018
E_f	1099
$\sigma_{el,g'\to g}$	2501

However, some parameters that are necessary for PDT are not included in the GENDF files for all isotopes, thus a python script was written to fill in the gaps for when parameters are missing from the GENDF file. For example, if $\chi(E)$ and ν are missing ^{234}U's GENDF file, we borrow the $\chi(E)$ from ^{235}U's GENDF file and we compute ν by dividing $\nu\sigma_f$ by σ_f. This may generate error in the quantity of interest, so any approximations made here must be noted.

In order to compute the variance for some quantity of interest with Barnfire, a PDT input file must be created manually and must declare that PDT is executed in adjoint

mode. Barnfire then runs a PDT simulation, using the input file and the FEDS cross section files, and generates an output file containing the sensitivities to the quantity of interest. Afterwards, Barnfire reads the PDT input, output, and cross sections files in order to create a python class containing necessary physical parameters and results from the simulation.

At this point, the ERRORR module of NJOY is used to generate a subelement covariance matrix for each isotope in the problem. Each subelement covariance matrix is condensed into a element covariance matrix via Eq.(2.15). Note that even if the element matrix is small, the subelement covariance matrix can be massive. Thus, looping over each element of the subelement covariance matrix and mapping that value over to the element covariance matrix can very computationally expensive. Instead, it is a better to create a mapping matrix beforehand, and use matrix multiplication to condense the subelement covariance matrix into the element covariance matrix. The mapping matrix is matrix containing values of zero or one, depending on whether a subelement j belongs to element i. Lastly, Eq.(2.14) is used to compute the variance in the quantity of interest.

4. BENCHMARK DESCRIPTIONS AND RESULTS

Four benchmark problems were used to test Barnfire's ability to generate cross sections and propagate uncertainties for FEDS, as well as compare Multigroup and FEDS error convergence rates in PDT. These four benchmarks included two verification problems, that were used to determine if Barnfire was correctly propagating uncertainties. This was done by comparing the estimate of the variance using Barnfire and PDT to the analytical solution for the variance. These benchmarks also included two validation problems, which were used to:

- compare convergence rates between contiguous and discontiguous energy grids
- verify that PDT's new triangle mesh generator works well for spherical problems
- verify that the uncertainty in the quantity of interest is within error margins of the experimental value for all problems

A description of each benchmark problem along with results are provided below.

4.1 Verification Problem 1

4.1.1 Description

The first verification problem is a pure-absorbing infinite-medium with an isotropic source of neutrons, where the quantity of interest Q is the reaction rate per unit volume, we can calculate Q by

$$Q = \langle \psi, q^{\dagger} \rangle$$

where $\langle \cdot, \cdot \rangle$ is an inner product over the relevant phase space,

$$\langle \cdot, \cdot \rangle \equiv \int_V dV \int_{4\pi} d\Omega \int_0^{\infty} dE$$

and

$$q^{\dagger} = \frac{\sigma_t}{V} \, .$$

We will now prescribe some arbitrary values for the source rate, cross sections, and the covariance matrix for a 2-element problem with 2 subelements within each element,

$$\begin{pmatrix} s_{t,1} \\ s_{t,2} \end{pmatrix} = \begin{pmatrix} 2 \\ 2 \end{pmatrix}$$

$$\begin{pmatrix} \sigma_1 \\ \sigma_2 \end{pmatrix} = \begin{pmatrix} 1 \\ 2 \end{pmatrix}$$

$$\text{cov}(\sigma_t, \sigma_t) = \begin{array}{c} \\ \sigma_{t,1,1} \\ \sigma_{t,2,1} \\ \sigma_{t,1,2} \\ \sigma_{t,2,2} \end{array} \begin{array}{c} \begin{array}{cccc} \sigma_{t,1,1} & \sigma_{t,2,1} & \sigma_{t,1,2} & \sigma_{t,2,2} \end{array} \\ \begin{pmatrix} 0.02 & 0.01 & 0 & 0 \\ 0.01 & 0.02 & 0.01 & 0 \\ 0 & 0.01 & 0.02 & 0.01 \\ 0 & 0 & 0.01 & 0.02 \end{pmatrix} \end{array}$$

$$\text{cov}(\sigma_s, \sigma_s) = \begin{array}{c} \\ \sigma_{s,1,1} \\ \sigma_{s,2,1} \\ \sigma_{s,1,2} \\ \sigma_{s,2,2} \end{array} \begin{array}{c} \begin{array}{cccc} \sigma_{s,1,1} & \sigma_{s,2,1} & \sigma_{s,1,2} & \sigma_{s,2,2} \end{array} \\ \begin{pmatrix} 0.02 & 0.01 & 0 & 0 \\ 0.01 & 0.02 & 0.01 & 0 \\ 0 & 0.01 & 0.02 & 0.01 \\ 0 & 0 & 0.01 & 0.02 \end{pmatrix} \end{array}$$

The subscripts for the σ's in the covariance matrices represent the element and it's subelement, respectively. Also, we will assume the source rate has no uncertainty in this problem.

4.1.2 Analytical Solution

For an infinite-medium FEDS transport equation reduces to

$$\Sigma_{t,e}(\hat{\Omega})\psi_e(\hat{\Omega}) = \sum_{\ell=0}^{\infty}\sum_{m=-\ell}^{\ell}\frac{2\ell+1}{4\pi}Y_\ell^m(\hat{\Omega})\sum_{e'=1}^{E}\Sigma_{s,\ell,e'\to e}\phi_{\ell,e'}^m + \frac{\chi_e}{4\pi}\sum_{e'=1}^{E}\nu\Sigma_{f,e'}\phi_{e'} + \frac{s_e}{4\pi} \quad (4.1)$$

where

$$\phi_{\ell,e'}^m = \int_{4\pi} d\Omega'\,\psi_{e'}(\hat{\Omega}')Y_\ell^m(\hat{\Omega}')\,.$$

However, since this problem has no fission source and isotropic scattering, Eq.(4.1) reduces to

$$\Sigma_{t,e}(\hat{\Omega})\psi_e(\hat{\Omega}) = \frac{1}{4\pi}\sum_{e'=1}^{E}\int_{4\pi} d\hat{\Omega}'\,\Sigma_{s,e'\to e}\psi_{e'}(\hat{\Omega}') + \frac{s_e}{4\pi}\,,$$

and by integrating over all 4π steradians,

$$\Sigma_{t,e}\phi_e = \sum_{e'=1}^{E}\Sigma_{s,e'\to e}\phi_{e'} + s_e\,. \quad (4.2)$$

This is a 2-element problem, therefore Eq.(4.2) splits up into two equations,

$$\Sigma_{t,1}\phi_1 = \Sigma_{s,1\to1}\phi_1 + \Sigma_{s,2\to1}\phi_2 + s_1 \quad (4.3a)$$

$$\Sigma_{t,2}\phi_2 = \Sigma_{s,1\to2}\phi_1 + \Sigma_{s,2\to2}\phi_2 + s_2\,. \quad (4.3b)$$

Furthermore, since there is only one material we can divide by the number density of the material to get

$$\sigma_{t,1}\phi_1 = \sigma_{s,1\to1}\phi_1 + \sigma_{s,2\to1}\phi_2 + s_1 \quad (4.4a)$$

$$\sigma_{t,2}\phi_2 = \sigma_{s,1\to2}\phi_1 + \sigma_{s,2\to2}\phi_2 + s_2\,. \quad (4.4b)$$

where s is now defined as the extraneous source rate divided by the number density. From Eq.(4.4b) it can shown that

$$\phi_2 = \frac{\sigma_{s,1\to 2}\phi_1 + s_2}{\sigma_{t,2} - \sigma_{s,2\to 2}}$$

and by plugging our new result for ϕ_2 into Eq.(4.4a) we obtain

$$\sigma_{t,1}\phi_1 = \sigma_{s,1\to 1}\phi_1 + \sigma_{s,2\to 1}\left[\frac{\sigma_{s,1\to 2}\phi_1 + s_2}{\sigma_{t,2} - \sigma_{s,2\to 2}}\right] + s_1$$

$$\phi_1\left\{\sigma_{t,1} - \sigma_{s,1\to 1} - \left[\frac{\sigma_{s,1\to 2}\sigma_{s,2\to 1}}{\sigma_{t,2} - \sigma_{s,2\to 2}}\right]\right\} = s_1 + \left[\frac{\sigma_{s,2\to 1}}{\sigma_{t,2} - \sigma_{s,2\to 2}}\right]s_2$$

$$\phi_1 = \frac{(\sigma_{t,2} - \sigma_{s,2\to 2})s_1 \ + \ \sigma_{s,2\to 1}s_2}{\sigma_{s,1\to 2}\sigma_{s,2\to 1} \ + \ (\sigma_{t,1} - \sigma_{s,1\to 1})(\sigma_{t,2} - \sigma_{s,2\to 2})} \tag{4.5}$$

Similarly, we can show that

$$\phi_2 = \frac{\sigma_{s,1\to 2}s_1 \ + \ (\sigma_{t,1} - \sigma_{s,1\to 1})s_2}{\sigma_{s,1\to 2}\sigma_{s,2\to 1} \ + \ (\sigma_{t,1} - \sigma_{s,1\to 1})(\sigma_{t,2} - \sigma_{s,2\to 2})} \tag{4.6}$$

From here, we can show that the quantity of interest,

$$Q = \sum_{e=1}^{E}\int_{4\pi} d\hat{\Omega}\,\psi_e\sigma_e \ ,$$

is equal to

$$Q = \frac{\sigma_{t,1}\big[(\sigma_{t,2} - \sigma_{s,2\to 2})s_1 \ + \ \sigma_{s,2\to 1}s_2\big] \ + \ \sigma_{t,2}\big[\sigma_{s,1\to 2}s_1 \ + \ (\sigma_{t,1} - \sigma_{s,1\to 1})s_2\big]}{\sigma_{s,1\to 2}\sigma_{s,2\to 1} \ + \ (\sigma_{t,1} - \sigma_{s,1\to 1})(\sigma_{t,2} - \sigma_{s,2\to 2})} \ . \tag{4.7}$$

Since we know this is pure absorber the quantity of interest simplifies to just

$$Q \ = \ s_1 + s_2 \ = \ 4$$

While the quantity of interest does not depend on σ_s, the sensitivities to the quantity of interest do depend on the values of $\sigma_{s,e'\to e}$. If one plugs in the numerical values for all the parameters in Eq.(4.7) except for $\sigma_{s,1\to1}$, one obtains the following equation for the quantity of interest.

$$Q = \frac{2\cdot 2 + 2(1-\sigma_{s,1\to1})2}{2(1-\sigma_{s,1\to1})}$$

$$Q = \frac{2}{1-\sigma_{s,1\to1}} + 2$$

Now by computing the sensitivity of Q to $\sigma_{s,1\to1}$ we get

$$\frac{\partial Q}{\partial \sigma_{s,1\to1}} = \frac{2}{(1-\sigma_{s,1\to1})^2}$$

$$\frac{\partial Q}{\partial \sigma_{s,1\to1}} = 2\,. \tag{4.8}$$

Similarly, for $\sigma_{s,1\to2}$

$$Q = \frac{2\cdot 2 + 2\cdot\sigma_{s,1\to2}\cdot 2 + 2}{2}$$

$$Q = 3 + 2\sigma_{s,1\to2}$$

$$\frac{\partial Q}{\partial \sigma_{s,1\to2}} = 2\,. \tag{4.9}$$

Similarly, for $\sigma_{s,2\to1}$

$$Q = \frac{2\cdot 2 + 2\sigma_{s,2\to1} + 2\cdot 2}{2}$$

$$Q = 4 + \sigma_{s,2\to1}$$

$$\frac{\partial Q}{\partial \sigma_{s,2\to1}} = 1\,. \tag{4.10}$$

Similarly, for $\sigma_{s,2\to2}$

$$Q = \frac{(2-\sigma_{s,2\to2})\cdot 2 + 2\cdot 2}{(2-\sigma_{s,2\to2})}$$

$$Q = 2 + \frac{4}{2 - \sigma_{s,2\to2}}$$

$$\frac{\partial Q}{\partial \sigma_{s,2\to2}} = \frac{4}{(2 - \sigma_{s,2\to2})^2}$$

$$\frac{\partial Q}{\partial \sigma_{s,2\to2}} = 1 \,. \tag{4.11}$$

Also, $\partial Q/\partial \sigma_{t,1} = \partial Q/\partial \sigma_{t,2} = 0$. Now using Eqs.(2.14) and (2.15), we can calculate the variance for a 2-element problem with 2 subelements per element as

$$\text{var}(Q) = \sum_{i=1}^{2}\sum_{j=1}^{2}\sum_{m=1}^{2}\sum_{n=1}^{2} \frac{\partial Q}{\partial p_i}\frac{\partial Q}{\partial p_j}\text{cov}(\theta_{i,m}, \theta_{j,n}) \,.$$

After plugging in all the appropriate values, the uncertainty in the quantity of interest is computed to be

$$\text{var}(Q) = 2.56 \,.$$

This is the value we hope to obtain from Barnfire. Note, this assumes there is no uncertainty in the covariance matrix values and that this is only a first-order estimate of the uncertainty in Q.

4.1.3 Results

The predefined cross sections and predefined covariance matrices were read by Barnfire's uncertainty quantification scripts. The results for Q and var(Q) provided by PDT and Barnfire are shown in Table 4.1.

Table 4.1: Comparison of Analytical Results to Barnfire for Verification Problem 1

	Analytical	Barnfire	Absolute Error
Q	4.0	4.0	0
var(Q)	2.56	2.56	-6.13×10^{-8}

These results confirmed that the uncertainty propagation routines are implemented correctly and can determine the variance of the reaction rate due to uncertainty in nuclear data.

4.2 Verification Problem 2

4.2.1 Description

The second verification problem is an isotropic-scattering infinite medium with a small fission source evenly-distributed in the medium. For simplification assume there are only 2 energy elements with 2 subelements in each element, where $\chi_1 = 1$, $\chi_2 = 0$, and

$$\begin{pmatrix} \sigma_{t,1} \\ \sigma_{t,2} \\ \nu\sigma_{f,1} \\ \nu\sigma_{f,2} \\ \sigma_{s,1\to1} \\ \sigma_{s,1\to2} \\ \sigma_{s,2\to1} \\ \sigma_{s,2\to2} \end{pmatrix} = \begin{pmatrix} 91 \\ 108 \\ 1 \\ 7 \\ 75 \\ 10 \\ 5 \\ 100 \end{pmatrix}$$

Now we'll prescribe some arbitrary values for the covariance matrix for a 2-element problem with 2 subelements within each element. We will assume that there are no cross-parameter covariances (note that this would not be true in a realistic problem because σ_t, $\nu\sigma_f$, and σ_s would in fact be correlated).

$$\text{cov}(\sigma_t, \sigma_t) = \begin{array}{c} \\ \sigma_{t,1,1} \\ \sigma_{t,2,1} \\ \sigma_{t,1,2} \\ \sigma_{t,2,2} \end{array} \begin{array}{c} \begin{array}{cccc} \sigma_{t,1,1} & \sigma_{t,2,1} & \sigma_{t,1,2} & \sigma_{t,2,2} \end{array} \\ \begin{pmatrix} 1.0 & 0.2 & 0 & 0 \\ 0.2 & 1.0 & 0.2 & 0 \\ 0 & 0.2 & 1.0 & 0.2 \\ 0 & 0 & 0.2 & 1.0 \end{pmatrix} \end{array}$$

$$\text{cov}(\nu\sigma_f, \nu\sigma_f) = \begin{array}{c} \\ \nu\sigma_{f,1,1} \\ \nu\sigma_{f,2,1} \\ \nu\sigma_{f,1,2} \\ \nu\sigma_{f,2,2} \end{array} \begin{array}{c} \begin{array}{cccc} \nu\sigma_{f,1,1} & \nu\sigma_{f,2,1} & \nu\sigma_{f,1,2} & \nu\sigma_{f,2,2} \end{array} \\ \begin{pmatrix} 1.0 & 0.2 & 0 & 0 \\ 0.2 & 1.0 & 0.2 & 0 \\ 0 & 0.2 & 1.0 & 0.2 \\ 0 & 0 & 0.2 & 1.0 \end{pmatrix} \end{array}$$

$$\text{cov}(\sigma_s, \sigma_s) = \begin{array}{c} \\ \sigma_{s,1,1} \\ \sigma_{s,2,1} \\ \sigma_{s,1,2} \\ \sigma_{s,2,2} \end{array} \begin{array}{c} \begin{array}{cccc} \sigma_{s,1,1} & \sigma_{s,2,1} & \sigma_{s,1,2} & \sigma_{s,2,2} \end{array} \\ \begin{pmatrix} 1.0 & 0.2 & 0 & 0 \\ 0.2 & 1.0 & 0.2 & 0 \\ 0 & 0.2 & 1.0 & 0.2 \\ 0 & 0 & 0.2 & 1.0 \end{pmatrix} \end{array}$$

In addition, we will set the quantity of interest to be the reactivity of the system

$$Q \;=\; \rho \;=\; \left(1 - \frac{1}{k}\right).$$

4.2.2 Analytical Solution

For a 2-element eigenvalue problem where $\chi_1 = 1$ and $\chi_2 = 0$, the transport equation simplifies to

$$\Sigma_{t,1}\phi_1 = \Sigma_{s,1\to1}\phi_1 + \Sigma_{s,2\to1}\phi_2 + \frac{1}{k}\Big(\nu\Sigma_{f,1}\phi_1 + \nu\Sigma_{f,2}\phi_2\Big) \tag{4.12a}$$

$$\Sigma_{t,2}\phi_2 = \Sigma_{s,1\to2}\phi_1 + \Sigma_{s,2\to2}\phi_2 \tag{4.12b}$$

From here we can show that

$$\frac{\phi_2}{\phi_1} = \frac{\sigma_{s,1\to2}}{\sigma_{t,2} - \sigma_{s,2\to2}}$$

and

$$Q \;=\; \Big(1 - \frac{1}{k}\Big) \;=\; 1 - \frac{\sigma_{t,1} - \sigma_{s,1\to1} - \sigma_{s,2\to1}\big(\frac{\sigma_{s,1\to2}}{\sigma_{t,2}-\sigma_{s,2\to2}}\big)}{\nu\sigma_{f,1} + \nu\sigma_{f,2}\big(\frac{\sigma_{s,1\to2}}{\sigma_{t,2}-\sigma_{s,2\to2}}\big)}\,. \tag{4.13}$$

After plugging in the corresponding values for all parameters we get that the medium is critical and reactivity is zero,

$$Q = 0\,.$$

The sensitivities of Q to all the parameters in this model are shown below. If one plugs in the numerical values for all the parameters in Eq.(4.13) except for $\sigma_{t,1}$, one obtains the following equation for the quantity of interest

$$Q = \frac{28}{3} - \frac{8}{78}\sigma_{t,1}\,.$$

Now by computing the sensitivity of Q to $\sigma_{t,1}$ we get

$$\frac{\partial Q}{\partial \sigma_{t,1}} = -\frac{8}{78}\,. \tag{4.14}$$

Similarly for $\sigma_{t,1}$ we get

$$Q = \frac{1170}{\sigma_{t,2} - 30}$$

$$\frac{\partial Q}{\partial \sigma_{t,2}} = -\frac{15}{78} \,. \tag{4.15}$$

For $\nu\sigma_{f,1}$ we get

$$Q = 1 - \frac{78}{8\nu\sigma_{f,1} + 70}$$

$$\frac{\partial Q}{\partial (\nu\sigma_{f,1})} = \frac{8}{78} \,. \tag{4.16}$$

For $\nu\sigma_{f,2}$ we get

$$Q = 1 - \frac{78}{8 + 10\nu\sigma_{f,2}}$$

$$\frac{\partial Q}{\partial (\nu\sigma_{f,2})} = \frac{10}{78} \,. \tag{4.17}$$

For $\sigma_{s,1\to1}$ we get

$$Q = \frac{8(\sigma_{s,1\to1} - 75)}{78}$$

$$\frac{\partial Q}{\partial \sigma_{s,1\to1}} = \frac{8}{78} \,. \tag{4.18}$$

For $\sigma_{s,1\to2}$ we get

$$Q = \frac{12(\sigma_{s,1\to2} - 10)}{7\sigma_{s,1\to2} + 8}$$

$$\frac{\partial Q}{\partial \sigma_{s,1\to2}} = \frac{12}{78} \,. \tag{4.19}$$

For $\sigma_{s,2\to1}$ we get

$$Q = \frac{10\sigma_{s,2\to1} - 50}{78}$$

$$\frac{\partial Q}{\partial \sigma_{s,2\to1}} = \frac{10}{78} \,. \tag{4.20}$$

For $\sigma_{s,2\to2}$ we get

$$Q = \frac{1100 - 15\sigma_{s,2\to2}}{\sigma_{s,2\to2} - 75}$$

$$\frac{\partial Q}{\partial \sigma_{s,2\to2}} = \frac{15}{78} \,. \tag{4.21}$$

Now using Eqs.(2.14) and (2.15), we can obtain the variance for a 2-element problem with 2 subelements per element,

$$\text{var}(Q) = \sum_{i=1}^{2}\sum_{j=1}^{2}\sum_{m=1}^{2}\sum_{n=1}^{2} \frac{\partial Q}{\partial p_i}\frac{\partial Q}{\partial p_j}\text{cov}(\theta_{i,m}, \theta_{j,n}) \,.$$

After plugging in all the appropriate values, the variance in the quantity of interest is computed to be

$$\text{var}(Q) = 0.4281 \,.$$

This is the value we hope to obtain from Barnfire.

4.2.3 Results

The predefined cross sections and predefined covariance matrices were read by Barnfire's uncertainty quantification scripts. The results for Q and var(Q) provided by PDT and Barnfire are shown in Table 4.2.

Table 4.2: Comparison of Analytical Results to Barnfire for Verification Problem 2

	Analytical	Barnfire	Absolute Error
Q	0	-1.01×10^{-8}	-1.01×10^{-8}
var(Q)	0.4281	0.4281	-5.33×10^{-8}

These results confirmed that Barnfire's uncertainty propagation routines are properly implemented for computing the variance in the reactivity ρ. These results increase our confidence that Barnfire would provide the right value for the variance in k_{eff} problems.

4.3 Validation Problem 1

4.3.1 Description

The first validation problem is an infinite medium of highly-enriched uranium (HEU), and the quantity of interest is the criticality factor k. Table 4.3 shows the concentration of uranium isotopes in the HEU.

Table 4.3: Concentration of isotopes in HEU.

isotope	number density $\left[\frac{\text{atoms}}{\text{barn-cm}}\right]$
^{234}U	4.9184×10^{-4}
^{235}U	4.4994×10^{-2}
^{238}U	2.4984×10^{-3}

Barnfire was used to generate FEDS, Multigroup, and continuous-energy cross sections for all three isotopes (with nuclear data from the ENDF/B-VII.1 cross section library). Afterwards, MCNP6 was used to compute the quantity of interest k.

The results from MCNP6 was considered to be "exact". The quantity of interest k was determined to be 2.26141 ± 0.00005. The neutron spectrum shown in Fig.(4.1) was computed in MCNP6 using a F4 tally along with the E0 card in order to create logarthmically-spaced energy bins. Afterwards, the neutron flux that MCNP6 tallied in each energy bin was divided by the bin width to obtain the flux in units of [n/cm^2-s-eV].

From Fig.(4.1) it is clear that the neutron spectrum in an infinite medium of HEU is a fast spectrum. The percentage of fissions caused by neutrons in the thermal (< 0.625 eV),

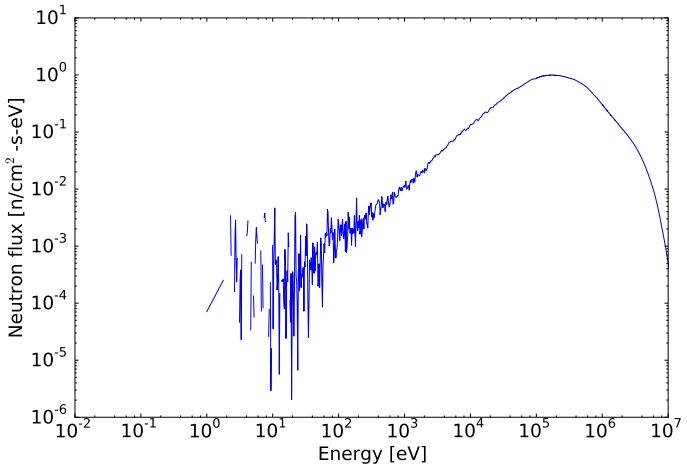

Figure 4.1: Neutron spectrum computed using MCNP6. Note that a lower neutron flux results in higher statistical noise.

intermediate (0.625 eV - 100 keV), and fast ($>$ 100 keV) energy ranges are 0.00%, 7.48%, and 92.52%, respectively. Thus the quantity of interest k will not be affected much by a slight variation in the thermal neutron flux. However, a slight variation in the fast neutron flux can have a strong impact on k.

The Multigroup and FEDS cross sections were tested separately using PDT, and the value of k was compared to the MCNP6's continuous-energy result. At the time this benchmark was tested, PDT was not able to read in double-differential fission cross sections $\Sigma_f(E' \rightarrow E)$. Instead, the fission source term was represented in terms of $\bar{\chi}(E)$, $\bar{\nu}(E)$, and $\Sigma_f(E)$. In order to compute an average fission spectrum $\bar{\chi}(E)$, we used the neutron spectrum generated by the MCNP6 simulation to weight the double-differential fission cross sections $\Sigma_f(E' \rightarrow E)$ and produce an accurate value for $\bar{\chi}(E)$. Whenever PDT is capable of handling double-differential fission cross sections, this step will no longer be required.

4.3.2 Results

Barnfire was used to decompose the resolved-resonance region of the energy domain into groups or elements for the Multigroup and FEDS simulations, as shown in Figures 4.2 and 4.3 respectively.

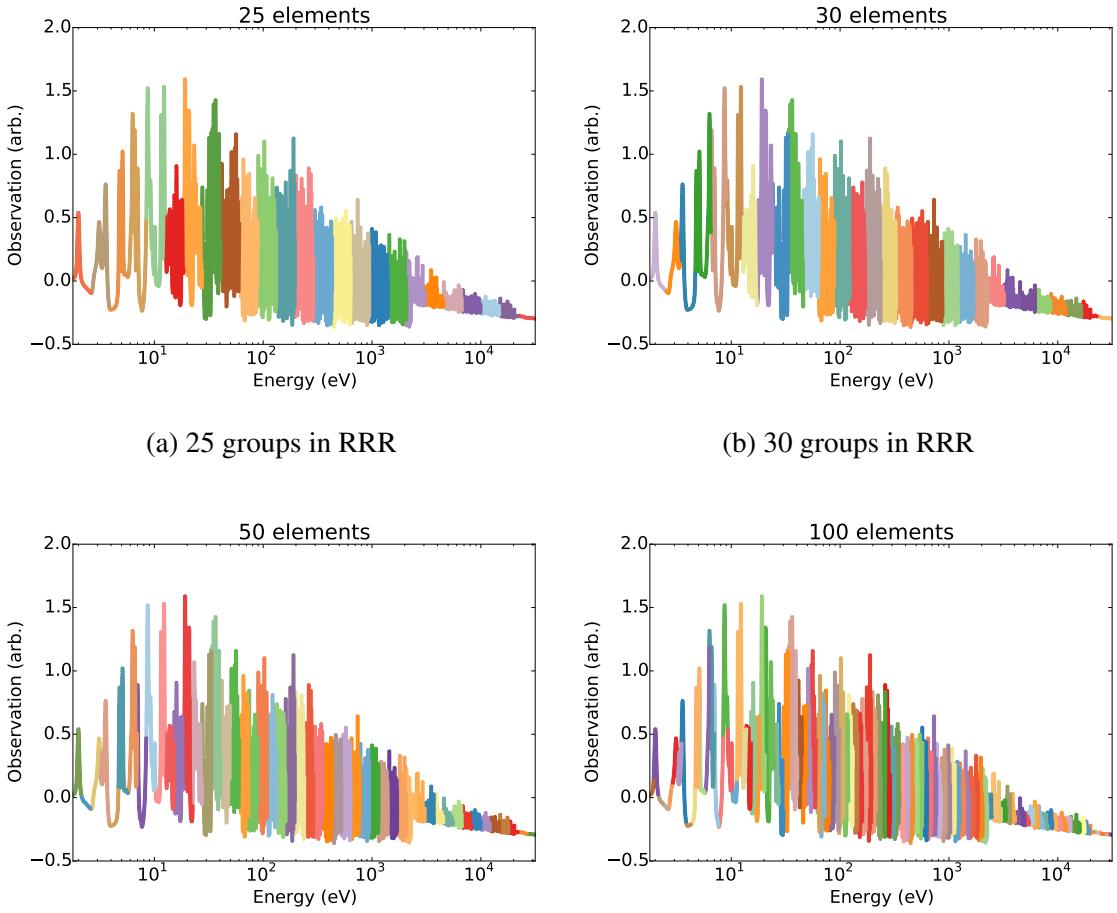

(a) 25 groups in RRR

(b) 30 groups in RRR

(c) 50 groups in RRR

(d) 100 groups in RRR

Figure 4.2: These plots demonstrate how Barnfire decomposes the resolved-resonance region (RRR) of the energy domain into logarithmically-spaced groups. Each color represents a different energy group.

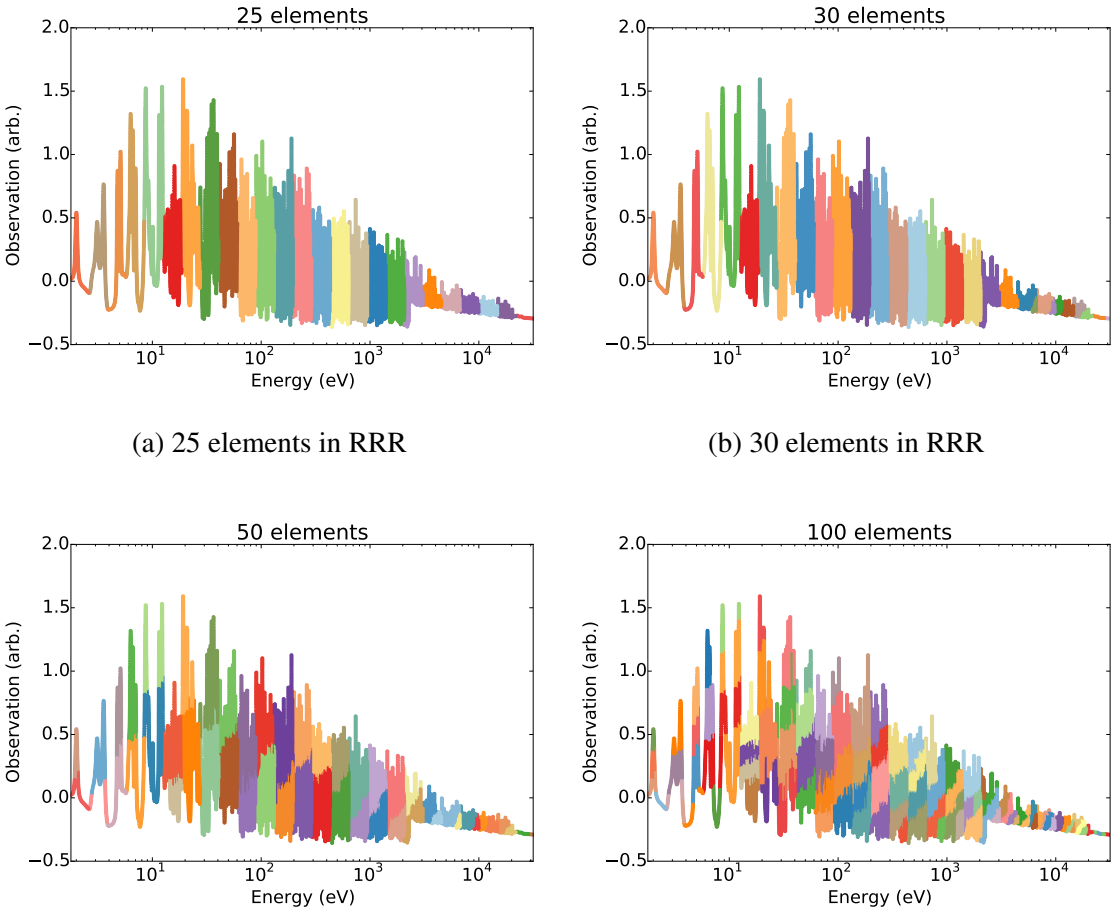

(a) 25 elements in RRR

(b) 30 elements in RRR

(c) 50 elements in RRR

(d) 100 elements in RRR

Figure 4.3: These plots demonstrate how Barnfire decomposes the resolved-resonance region (RRR) into 25 logarithmically-spaced coarse-groups, and add elements to the 25 coarse-groups by arbitrarily clustering energy segments within the coarse-groups into elements. Each color represents a different energy element.

The contiguous and discontiguous energy grids generated by Barnfire were used for separate PDT simulations. The neutron spectra generated by PDT for different number of groups in the resolved-resonance region (RRR) is shown in Fig.(4.4), and the neutron spectra generated by PDT for different number of elements in the RRR in Fig.(4.5).

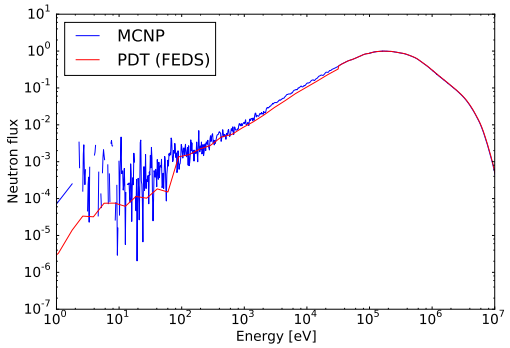

(a) 25 groups in RRR

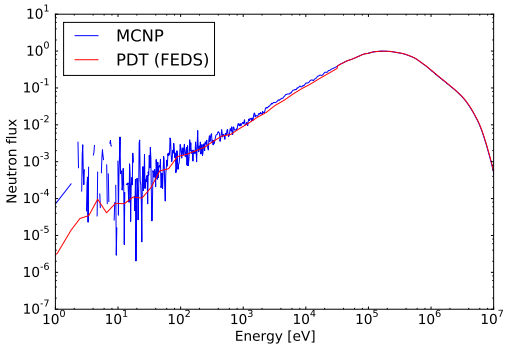

(b) 30 groups in RRR

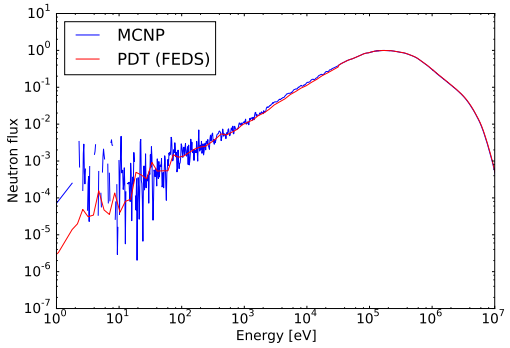

(c) 50 groups in RRR

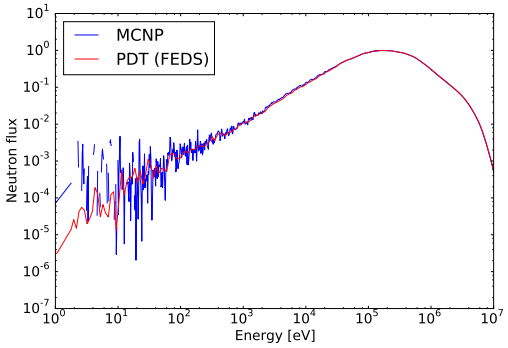

(d) 100 groups in RRR

Figure 4.4: Comparison of Multigroup neutron spectra in PDT to a continuous-energy neutron spectrum in MCNP. Each PDT Multigroup simulation contained 14 groups in the thermal region ($<$ 1.7 eV) and 250 groups in the URR ($>$ 31 keV). The number of groups in the RRR was varied from 25 to 100 groups.

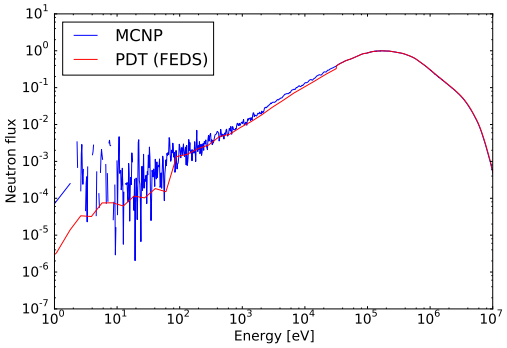

(a) 25 elements in RRR

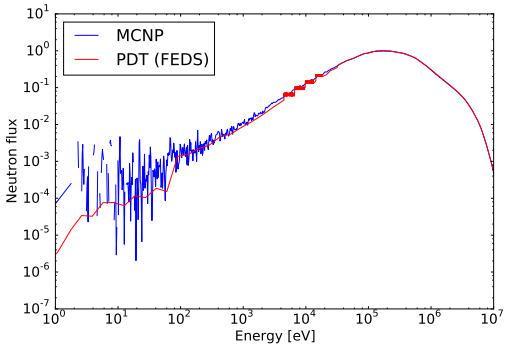

(b) 30 elements in RRR

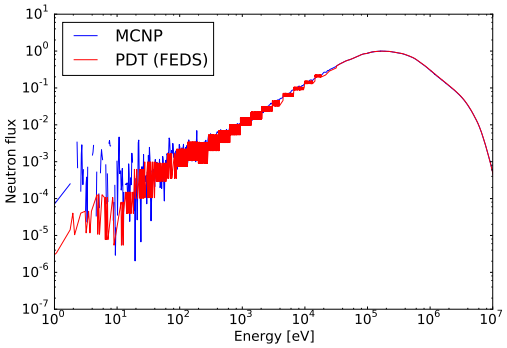

(c) 50 elements in RRR

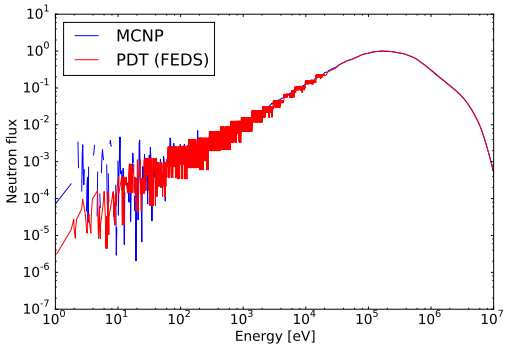

(d) 100 elements in RRR

Figure 4.5: Comparison of FEDS neutron spectra in PDT to a continuous-energy neutron spectrum in MCNP. Each PDT FEDS simulation contained 14 groups in the thermal region (< 1.7 eV) and 250 groups in the URR (> 31 keV). The number of elements in the RRR was varied from 25 to 100 elements.

Due to the fact that an infinite medium of HEU generates a fast neutron spectrum, only 14 energy groups were needed in the thermal region. We compared using 14 groups in the thermal region to using 49 groups in the thermal region with PDT and they both yielded the same value for k_{eff}, to within 10^{-7}. Thus we concluded 14 groups was a sufficient number of groups for the thermal region. However, we were not sure how many groups would be necessary for the unresolved-resonance region (URR) of the energy domain. We tested the FEDS with a variable number of URR groups. Table 4.4 shows the FEDS energy grid that was used for this particular study, and Figure 4.6 depicts how k_{eff} converges as the number of groups in the URR is increased.

Table 4.4: Energy grid used for URR convergence study

Energy Region	Number of Elements
thermal energy region ($<$ 1.7eV)	14
resolved resonance region (1.7eV —31keV)	50
unresolved resonance region ($>$ 31keV)	*variable*

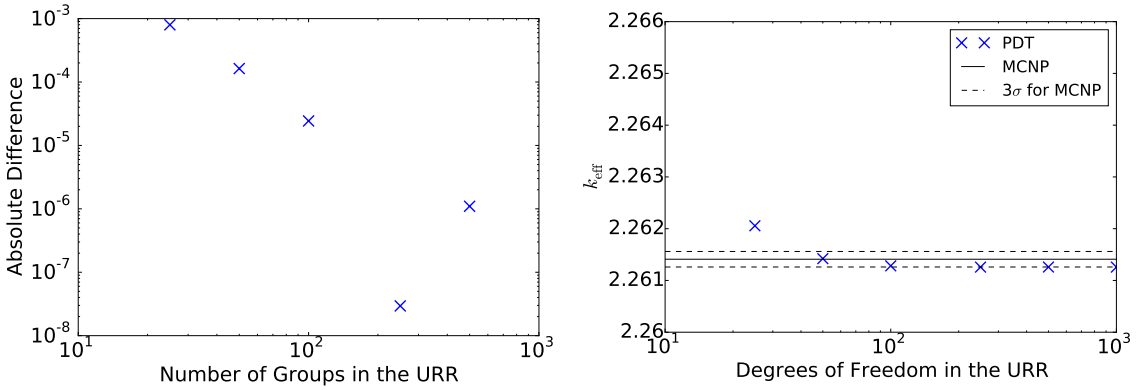

(a) (b)

Figure 4.6: Energy-discretization convergence of k_{eff} for Multigroup and FEDS. Plot (a) shows how far the Multigroup and FEDS solutions are from a reference converged solution (the reference solution in this case is the value k_{eff} when using 1000 groups in the URR). Plot (b) demonstrates how the FEDS value for k_{eff} quickly falls within 3 standard deviations of the continuous-energy MCNP6 solution.

Results were considered converged when the absolute difference between k_{eff} and a *reference result* was less than 10^{-5}. The reference result in this case was the value for k_{eff} when 1000 groups were used in the URR. According to this study, using 250 groups in the URR was sufficient.

Next, we compared the convergence rate of k_{eff} between using Multigroup and FEDS in the resolved-resonance range (RRR). Table 4.5 shows the energy grid that was used for this particular study. Figure 4.7 compares the convergence rates between FEDS and Multigroup.

Table 4.5: Energy grid used for Validation Problem 1 PDT simulations

Energy Range	Number of Elements
thermal energy region ($<$ 1.7eV)	14
resolved resonance region (1.7eV —31keV)	*variable*
unresolved resonance region ($>$ 31keV)	250

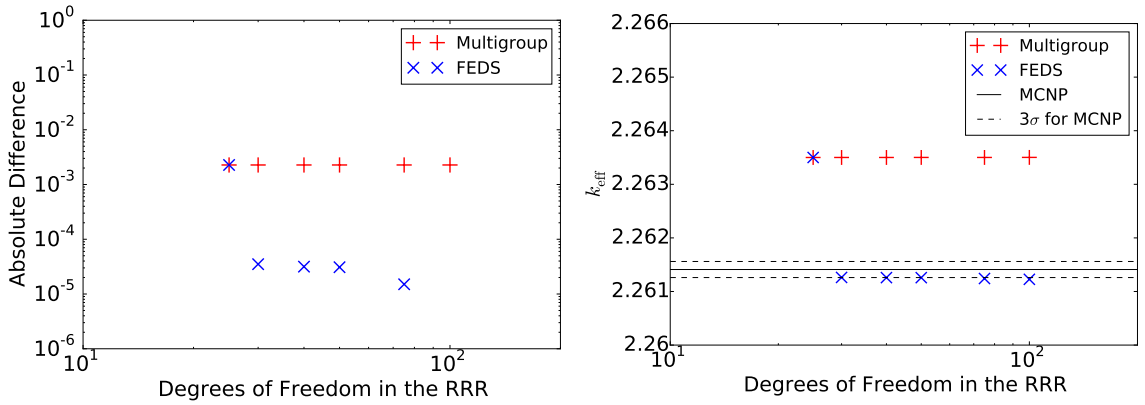

(a) (b)

Figure 4.7: Energy-discretization convergence of k_{eff} for Multigroup and FEDS. Plot (a) shows how far the Multigroup and FEDS solutions are from a reference converged solution (the reference solution in this case is the FEDS value for k_{eff} when using 100 elements in the RRR). Plot (b) demonstrates how the FEDS value for k_{eff} quickly falls within 3 standard deviations of the continuous-energy MCNP6 solution.

As shown in Fig.(4.7), FEDS converges very quickly to the continuous-energy solution, while the Multigroup method converges very slowly for this problem. We hypothesize that the reason FEDS slightly diverges from the continuous-energy solution when a large number of elements is used in the RRR is that we set a minimum subelement-width size. Namely, the upper energy bound for a subelement had to be at least 1.0001 times larger than the lower energy bound for that subelement. Setting this minimum subelement-width prevents ERRORR from crashing, however it may not allow Barnfire to cluster subelements properly and may explain why the accuracy of FEDS is hindered as more energy elements are used in the RRR.

Afterwards, we used Barnfire to propagate the error from the ENDF/B-VII.1 nuclear data library to determine the variance in k_{eff} due to nuclear data uncertainty for the Multigroup and FEDS simulations. We then took the square root of the variance for each simulation to determine the standard deviation. Figure 4.8 shows the standard deviation for each simulation as a function of degrees of freedom in the RRR.

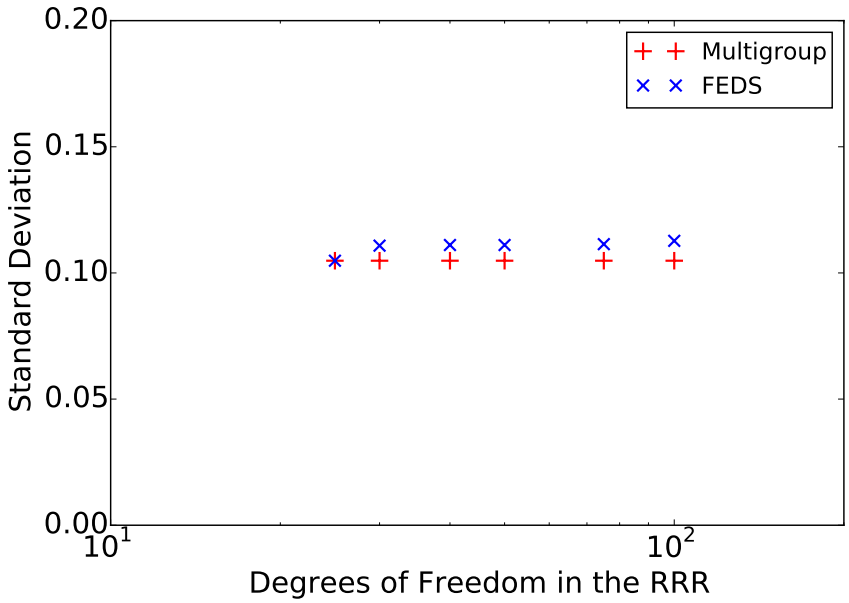

Figure 4.8: Standard deviation due to nuclear data uncertainty for different Multigroup and FEDS simulations.

When using the Multigroup method, the variance in k_{eff} remains constant as more energy group are added to the RRR. However when using FEDS, the variance just slightly increases as more energy elements are added to the RRR. Note that Fig.(4.8) does not include discretization error (which decreases when a finer energy grid is used), it only includes error due to uncertainty of different nuclear reaction cross sections for ^{234}U, ^{235}U, and ^{238}U. Also, note that Barnfire is not a heavily-benchmarked code. Our confidence that these standard deviation estimates are accurate rest on the success of Verification Problems 1 and 2 in this document.

4.4 Validation Problem 2

4.4.1 Description

The second validation problem is probably the most famous nuclear engineering benchmark problem, Godiva, a sphere of HEU with a radius of 8.7407 cm. Experimentally, the

criticality factor k for Godiva is exactly one. This benchmark problem is the same as Validation Problem 1 except the geometry is spherical, so please refer to the description of Validation Problem 1 for problem specifications that are not related to this problem's geometry.

Currently, PDT only has two options for spatial discretization: a 3D Cartesian mesh, or a triangular mesh in the X-Y plane which can be extruded along the Z axis to create a 3D geometry. For this benchmark, PDT's triangular mesh was used to approximate the sphere of HEU, as shown in Figure 4.9.

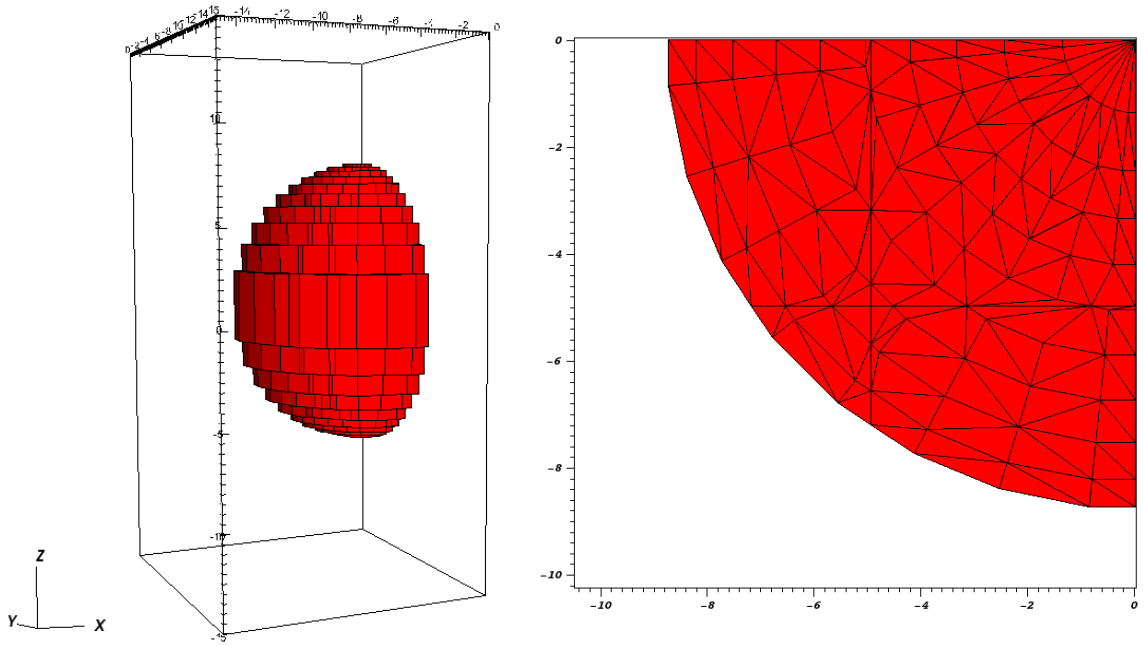

Figure 4.9: A 32-sided polygon in the X-Y plane, extruded into 19 "stair steps" along the Z axis was constructed in order to approximate Godiva (left). A triangular mesh was used to construct the 32-sided polygon, and cut-planes were used to decomposes the geometry (right).

4.4.2 Results

Due to computational resource constraints we did not run a Godiva simulation that was fully resolved in space, energy and angle. Table 4.6 outlines the levels of discretization that were used in this study.

Table 4.6: Energy grid used for Validation Problem 2 PDT simulations

Domain Type	Discretized Portion of Domain	Discretization
Space	X-Y plane	32-sided polygon
	Z axis	19 "stair steps"
Energy	thermal energy region ($<$ 1.7eV)	14 Groups
	resolved resonance region (1.7eV —31keV)	*variable*
	unresolved resonance region ($>$ 31keV)	250 Groups
Angle	S_N quadrature angles per octant	16 Angles
	highest Legendre moment for scattering kernel	3rd moment

Figures 4.10 and 4.11 illustrate how Barnfire decomposed the resolved-resonance region of the energy domain for the Multigroup and FEDS Godiva-simulations.

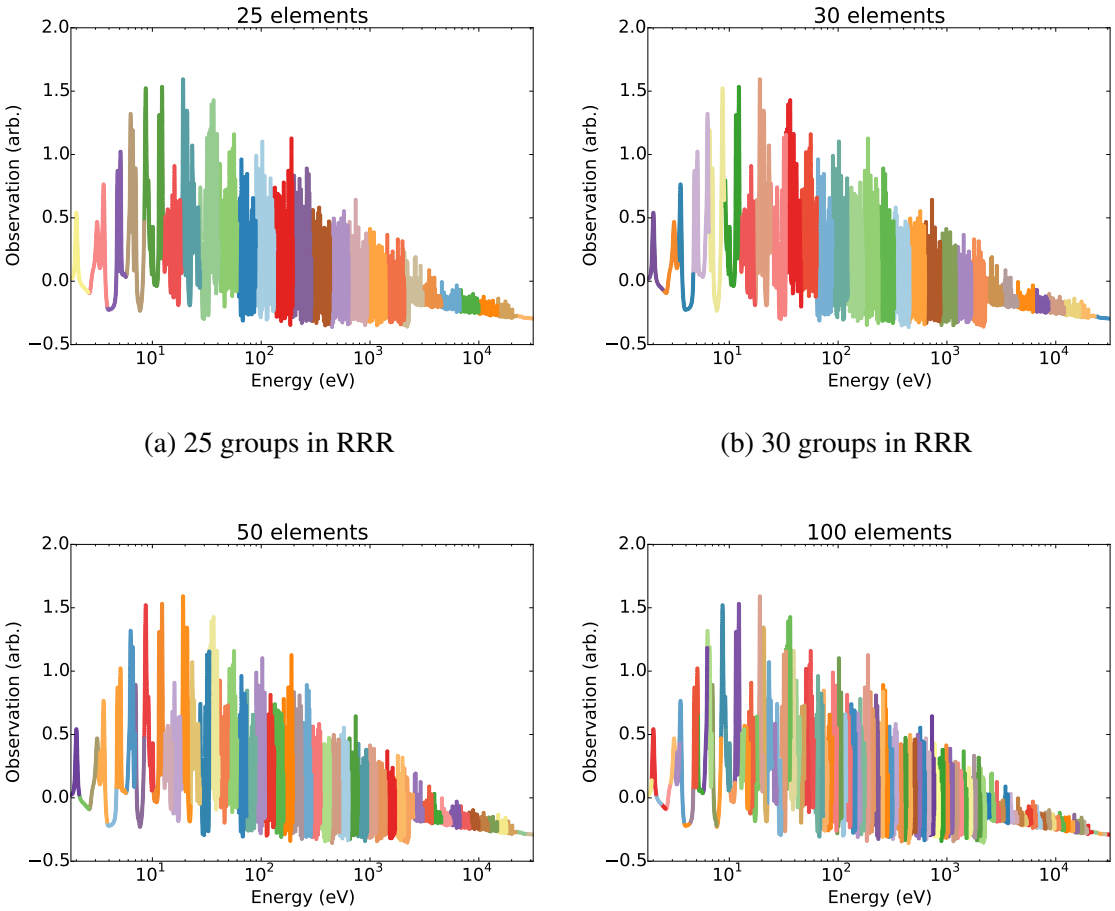

(a) 25 groups in RRR

(b) 30 groups in RRR

(c) 50 groups in RRR

(d) 100 groups in RRR

Figure 4.10: These plots demonstrate how Barnfire decomposes the resolved-resonance region (RRR) of the energy domain into logarithmically-spaced groups. Each color represents a different energy group.

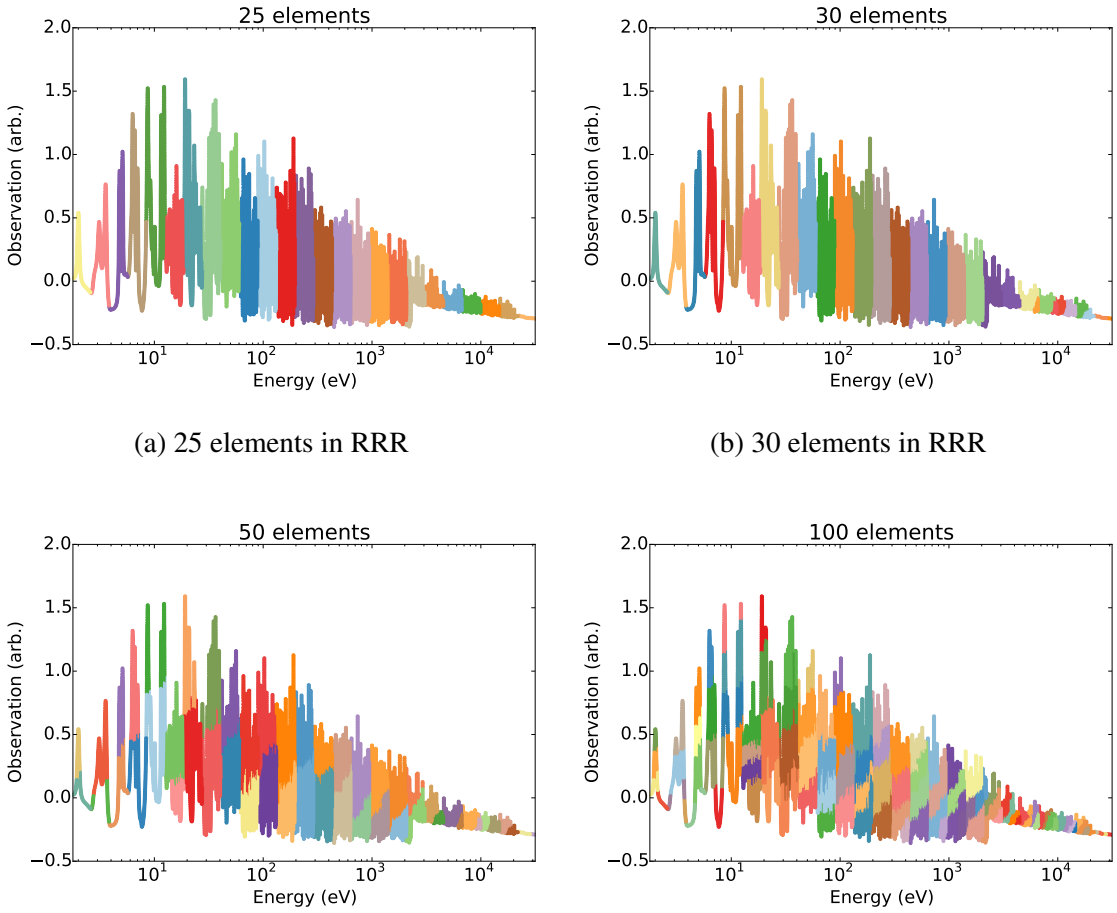

(a) 25 elements in RRR

(b) 30 elements in RRR

(c) 50 elements in RRR

(d) 100 elements in RRR

Figure 4.11: These plots demonstrate how Barnfire decomposes the resolved-resonance region (RRR) into 25 logarithmically-spaced coarse-groups, and add elements to the 25 coarse-groups by arbitrarily clustering energy segments within the coarse-groups into elements. Each color represents a different energy element.

Using the different Multigroup and FEDS energy grids, we were able to compare the convergence rates of k_{eff} for Godiva, as depicted by Figure 4.12. While Fig.(4.12a) shows FEDS converging faster than Multigroup method, Fig.(4.12b) shows neither method approaches the experimental value of $k_{\text{eff}} = 1$. The majority of the discrepancy in k_{eff} is likely due to spatial-discretization error. A MCNP6-to-PDT geometry converter was used

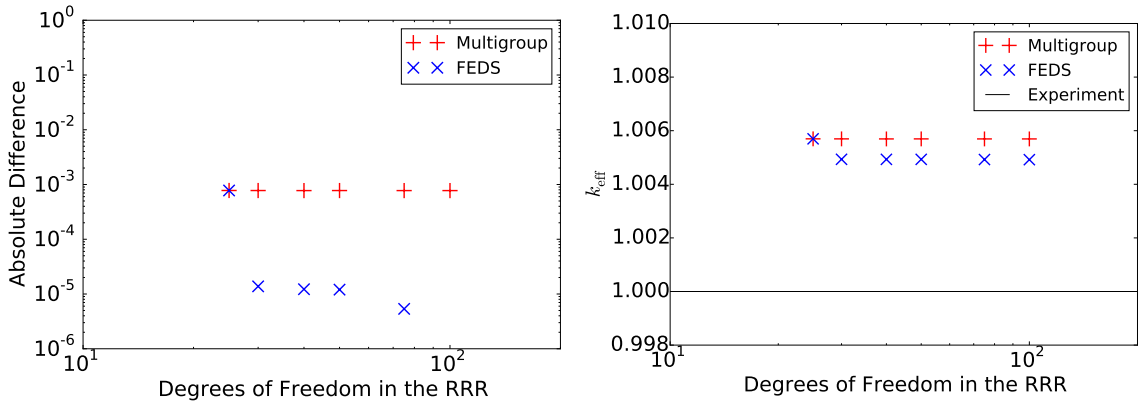

(a) (b)

Figure 4.12: Energy-discretization convergence of k_{eff} for Multigroup and FEDS. Plot (a) shows how far the Multigroup and FEDS solutions are from a reference converged solution (the reference solution in this case is the FEDS value for k_{eff} when using 100 elements in the RRR). Plot (b) demonstrates how the FEDS value for k_{eff} quickly falls within 3 standard deviations of the continuous-energy MCNP6 solution.

to approximate the MCNP6 geometry. The converter is supposed to preserve the original volume of the geometry, however this was never verified. In addition, the level of discretization is very coarse.

Based on the results from Validation Problem 1, we expect the energy-discretization error to be 2×10^{-4}. Also, based on a few angular-discretization convergence studies we expect the error due to using 16 S_N quadrature angles per octant and a P_3 scattering kernel approximation to be $O(10^{-4})$ and $O(10^{-5})$, respectively. By process of elimination, this further verifies that the spatial-discretization error is likely the dominant source of error in this problem.

5. CONCLUSION

To summarize, the FEDS is a generalized finite element framework for energy discretization that decomposes the energy domain into coarse groups and then further partitions the coarse groups into discontiguous energy elements. A cross section generation framework, Barnfire, was updated in order to generate cross sections and propagate uncertainties for Multigroup and FEDS to simulate fast spectrum problems. Barnfire was also updated to allow the user to control the subelement-width size, compute accurate escape cross sections in finite geometries, and customize the weighting spectrum for a larger variety of radiation transport problems.

Two verification problems were simulated using Barnfire and PDT. The results confirmed that Barnfire's uncertainty quantification scripts were able to accurately propagating the error from the ENDF nuclear data library onto the quantity of interest. Barnfire computed the quantity of interest and variance to within 10^{-7} from the analytical value for both verification problems.

Afterwards, two validation problems were used to test Barnfire. The first problem was an infinite medium of HEU, with k_{eff} as the quantity of interest. It demonstrated that FEDS was able to converge much faster than Multigroup to the "exact" solution as finer energy meshes were used. The absolute error with a resolved energy mesh (14 groups in the thermal range, 100 FEDS elements in the RRR, and 250 groups in the URR) was 2×10^{-4}, but with a standard deviation of 0.12 due to nuclear data uncertainty. The second problem was a sphere of HEU, with k_{eff} as the quantity of interest. Once again, it demonstrated that FEDS converged much faster the Multigroup method, but the smallest absolute error that was achieved was 4×10^{-3}.

The results from these benchmark problems suggest that Barnfire is producing accu-

rate FEDS cross sections, correctly propating uncertainties from the nuclear data libraries, and that FEDS converges faster than Multigroup to an energy-resolved solution. Future work, on this topic includes increasing the level of angular and spatial refinement and reattemping the second validation problem.

REFERENCES

[1] A. T. Till, *Master of Science Thesis Proposal: A Generalized Multigroup Method*. PhD thesis, Texas A&M University, 2013.

[2] M. Nikolaev and V. Filippov, "Measurement of the resonance parameters for total cross sections of some elements in the energy region 0.3-2.7 mev," *Atom. Energ*, vol. 6, no. 6, 1963.

[3] V. Sinitsa and M. Nikolaev, "Analytical determination of subgroup parameters," *Sov. At. Energy (Engl. Transl.), v. 35, no. 6, pp. 1129-1131*, 1973.

[4] J. Sinitsa, "Non-grey radiative transfer," *J. Quant. Spectrosc. Radiat. Transfer 4, pp. 723-729*, 1964.

[5] A. T. Till, *Finite Elements with Discontiguous Support for Energy Discretization in Particle Transport*. PhD thesis, Texas A&M University, 2015.

[6] D. E. Bruss, *Adjoint-Based Uncertainty Quantification for Neutron Transport Calculations*. PhD thesis, Texas A&M University, 2016.

[7] D. Muir, R. Boicourt, and A. Kahler, "The njoy nuclear data processing system, version 2012," tech. rep., LA-UR-12-27079, 2012.

[8] A. N. M. Mathis, Mark M. and M. L. Adams, "A general performance model for parallel sweeps on orthogonal grids for particle transport calculations," tech. rep., Department of Computer Science, Texas A&M University, 2000.

[9] J. T. Goorley, M. R. James, T. E. Booth, F. Brown, J. Bull, L. J. Cox, J. Durkee, J. Elson, M. Fensin, R. Forster, *et al.*, "Initial mcnp6 release overview-mcnp6 version 1.0," tech. rep.

[10] H. F. Stripling, *Adjoint-Based Uncertainty Quantification and Sensitivity Analysis for Reactor Depletion Calculations*. PhD thesis, Texas A&M University, 2013.